Estimating the Top Altitude of Optically Thick Ice Clouds from Thermal Infrared Satellite Observations Using CALIPSO Data

Patrick Minnis[1], Chris R. Yost[2], Sunny Sun-Mack[2], and Yan Chen[2]

[1]NASA Langley Research Center, Hampton, VA, USA

[2]Science Systems and Applications, Inc., Hampton, VA, USA

Revision for *Geophysical Research Letters*

April 2008

Abstract

The difference between cloud-top altitude Z_{top} and infrared effective radiating height Z_{eff} for optically thick ice clouds is examined using April 2007 data taken by the Cloud-Aerosol Lidar and Infrared Pathfinder Satellite Observations (CALIPSO) and the Moderate-Resolution Imaging Spectroradiometer (MODIS). For even days, the difference ΔZ between CALIPSO Z_{top} and MODIS Z_{eff} is 1.58±1.26 km. The linear fit between Z_{top} and Z_{eff}, applied to odd-day data, yields a difference of 0.03±1.21 km and can be used to estimate Z_{top} from any infrared-based Z_{eff} for thick ice clouds. Random errors appear to be due primarily to variations in cloud ice-water content (IWC). Radiative transfer calculations show that ΔZ corresponds to an optical depth of ~1, which based on observed ice-particle sizes yields an average cloud-top IWC of ~0.015 gm^{-3}, a value consistent with in situ measurements. The analysis indicates potential for deriving cloud-top IWC using dual-satellite data.

1. Introduction

Spectral bands in the infrared (IR) atmospheric window (10-12 μm) are routinely used to estimate cloud top heights from passive satellite sensors [e.g., *Rossow and Schiffer*, 1999; *Minnis et al.*, 1995]. IR radiation is relatively transparent to the atmosphere above the cloud, and the observed 11-μm brightness temperature T_{11} can be matched to local temperature soundings to find the cloud height. Although it is recognized that the effective radiating temperature of optically thin clouds corresponds to some level below cloud top, it is commonly assumed that optically thick clouds have sharp boundaries and optically thick edges. They are generally treated as blackbodies, and so T_{11} is assumed to be equivalent to the cloud-top temperature plus a small correction for atmospheric absorption and cloud particle scattering. Recent research has demonstrated, however, that even deep convective clouds do not have such sharply defined boundaries in the IR spectrum. For example, *Sherwood et al.* [2004] found that cloud tops derived from the eighth Geostationary Operational Environmental Satellite (GOES-8) were 1-2 km below the convective cloud tops detected by lidar data collected over Florida. Those and other results require new approaches to interpret the infrared brightness temperatures of optically thick clouds. Measurements from active sensors combined with passive infrared radiances are needed to address this outstanding problem.

Until recently, active remote sensing of optically thick clouds has been extremely limited. Ground-based radars and lidars profile the atmosphere continuously, but observe at only one location. They are also unlikely to detect the physical tops of optically thick ice clouds because lidars can only penetrate to optical depths of less than about 3 into the cloud and cloud radars often have no returns from smaller ice crystals common at the tops of such clouds. Active sensors aboard aircraft can sample a larger area during field campaigns and can outline the tops

54 of the clouds, but they collect data for only a few days over the duration of a given experiment.
55 With the 2006 launch of the Cloud-Aerosol Lidar and Infrared Pathfinder Satellite Observations
56 (CALIPSO) satellite into orbit behind the *Aqua* satellite in the A-Train, coincident and nearly
57 simultaneous global lidar and infrared radiance measurements are now available. This study uses
58 the measurements from CALIPSO and the *Aqua* Moderate-Resolution Imaging
59 Spectroradiometer (MODIS) to develop a new method to estimate the physical top of optically
60 thick ice clouds from passive IR imager data.
61
62 **2. Data and Methodology**
63 Like *Aqua*, CALIPSO follows a Sun-synchronous orbit with an approximately 1330-LT
64 equatorial crossing time ~90 s behind *Aqua*. Because CALIPSO is offset by 7-18° east of *Aqua*,
65 the *Aqua* sensors typically observe the CALIPSO ground track at viewing zenith angles VZA of
66 9-19°. The primary instrument on CALIPSO is the Cloud Aerosol Lidar with Orthogonal
67 Polarization (CALIOP), which has 532 and 1064-nm channels for profiling clouds and aerosols
68 [*Winker et al.*, 2007]. The CALIOP footprints are nominally 70-m wide and sampled every 330
69 m. This instrument allows the global characterization of cloud vertical structure with vertical
70 resolutions up to 30 m. The CALIPSO data used here are the April 2007 Version 1.21 1/3 km
71 cloud height products [*Vaughan et al*., 2004].
72 Cloud properties derived from 1-km *Aqua* MODIS radiances using the Clouds and the
73 Earth's Radiant Energy System (CERES) project cloud retrieval algorithms [*Minnis et al.*, 2006]
74 were matched with CALIOP data (see *Sun-Mack et al.* [2007]). The CERES cloud properties are
75 determined from the radiances using updated versions of the daytime Visible Infrared Solar-
76 Infrared Split Window Technique (VISST) and the nighttime Solar-infrared Infrared Split-

77 window Technique (SIST) [*Minnis et al.*, 1995]. The products include cloud temperature, height,
78 thermodynamic phase, optical depth, effective ice crystal diameter D_e, and other cloud
79 properties.

80 The VISST/SIST first determines the effective radiating temperature T_{eff}, which
81 corresponds to a height somewhere within the cloud Z_{eff} [e.g., *Minnis et al.*, 1990]. For clouds
82 above 500 hPa, Z_{eff} is determined by matching T_{eff} to a local atmospheric temperature sounding.
83 For optically thin ice clouds, an empirical correction is applied to estimate the true cloud-top
84 temperature T_{top} based on cloud emissivity [*Minnis et al.*, 1990]. The cloud-top altitude Z_{top} for
85 those clouds is the lowest level in the sounding corresponding to T_{top}. Optically thick clouds are
86 assumed to have sharp boundaries and, therefore, most IR radiation reaching the satellite sensor
87 is emitted by the uppermost part of the cloud. In optically thick cases, VISST and SIST assume
88 that T_{eff} is equivalent to T_{top} and $Z_{top} = Z_{eff}$. VISST accounts for the effects of infrared scattering
89 effects so, for these clouds, T_{eff} is slightly greater than T_{11}.

90 Matched VISST and CALIPSO data from every even day during April 2007 were
91 selected to develop a relationship between the effective and physical cloud-top heights of
92 optically thick ice clouds. Clouds with effective emittance exceeding 0.98 (visible optical depth τ
93 > 8) are considered to be optically thick. This definition includes a wide variety of clouds
94 including thick cirrus and convective cloud anvils and cores. Polar clouds (latitudes > 60°) were
95 excluded to avoid mischaracterizing them over ice and snow. The method is tested using the odd-
96 day April 2007 MODIS-CALIPSO non-polar matched data.

97 **3. Cloud-Top Height Correction**

98 Figure 1 shows CALIOP backscatter intensity profiles (Figure 1a) and scene
99 classifications for a 1-h segment of a 27 April 2007 CALIPSO orbit. It began in darkness over

North America, crossed the Pacific and Antarctica into daylight, and ended in the Indian Ocean. The scene classifications (Figure 1b), which show cloud and aerosol locations, are overlaid with black dots corresponding to Z_{top} from CERES-MODIS for optically thick, single-layer ice clouds. These are evident as the gray areas underneath the clouds. The absence of black dots indicates that the cloud is liquid water, multilayered, or optically thin cirrus. Generally, Z_{top} is 1-2 km below the CALIPSO top Z_{topCAL}.

The cloud-top height pairs for all even days during April 2007 are plotted in Figure 2 as density scatter plots with linear regression fits. In Figure 2a, the average difference between the 15,367 Z_{topCAL} and their Z_{eff} pairs increases slightly with increasing altitude. The mean difference, Z_{eff} - Z_{topCAL}, is -1.58 ± 1.26 km. The linear regression fit plotted over the data,

$$Z_{top} = 1.094\, Z_{eff} + 0.751 \text{ km}, \qquad (1)$$

yields a squared linear correlation coefficient $R^2 = 0.89$. According to Eq(1), the difference ΔZ between Z_{top} and Z_{eff} rises from ~1.25 km for $Z_{eff} = 5$ km up to more than 2 km for $Z_{eff} > 14$ km.

Applying Eq(1) to Z_{eff} in Figure 1b yields the new values in Figure 1c that are mostly very close to the corresponding Z_{topCAL}. Figure 2b compares the 15,170 values of Z_{topCAL} and Z_{top} computed with Eq (1) for all April 2007 odd-day data. The data corresponding to $Z_{topCAL} > 3$ km are centered along the line of agreement, while lower cloud heights are overestimated. The correction yields a mean difference of -0.03 ± 1.21 km and the results are more correlated than the even-day data, having $R^2 = 0.91$. This empirical correction effectively eliminates the bias and slightly reduces the random error in the estimated Z_{top}. The correction is robust in that it applies

well to two independent datasets. The Z_{top} estimates were not constrained to be below the tropopause.

For Z_{eff} < 3 km, the data tend to be centered on the line of agreement in Figure 2a indicating that no correction is needed. The correction results in unphysical values at those altitudes and should not be applied. This overestimation is due to uncertainties in the atmospheric profile of temperature in the lower layers (e.g., *Dong et al.* [2008]) or to the misclassification of supercooled-liquid water or mixed-phase clouds as ice clouds by the CERES-MODIS *Aqua* algorithm. The basic assumption that the correction is for ice clouds would be violated for those and other low-level pixels. The tops of water clouds are unlikely to be more than a few hundred meters above Z_{eff} [e.g., *Dong et al.*, 2008]. For low clouds, a better estimate of Z_{eff} and a more accurate phase classification are needed before applying a correction to obtain Z_{top}. That effort is beyond the scope of this paper.

To minimize the impact of low-altitude temperature and phase uncertainties in the retrievals, the regression was also performed using the even-day data (13,046 samples) only for ice clouds with effective pressures, p_{eff} < 500 hPa. The resulting fit is

$$Z_{top} = 1.041\, Z_{eff} + 1.32 \text{ km}. \qquad (2)$$

Applying Eq (2) to odd-day clouds having p_{eff} < 500 hPa yields an average difference of -0.08 ± 1.15 km. This difference is nearly the same as the average difference of -0.13 ± 1.14 km that would be obtained by applying Eq (1) to the same odd-day dataset. If Eq (2) is used to estimate Z_{top} for *all* of the odd-day data, the mean difference is 0.07 ± 1.24 km. The results are essentially

144 the same for both fits. The 500-hPa cutoff effectively eliminates the low-cloud heights that
145 would be overestimated by estimating Z_{top} from Z_{eff} with either correction.
146
147 **4. Discussion**
148 The instantaneous differences can mainly be attributed to uncertainties in the temperature
149 profiles used to convert temperature to altitude, spatial mismatches in the data, VZA
150 dependencies, and variations in cloud microphysics. The small portions of the satellite pixel
151 sampled by the narrow lidar footprint can cause some significant differences if cloud height
152 varies within the pixel. Errors in the temperature profiles can move Z_{eff} up or down. For example,
153 some of the Z_{eff} values between 6 and 14 km in Figure 2a are lower than the corresponding
154 values of Z_{topCAL} and account for ~ 1 km of the range in ΔZ. It could also account for some of the
155 extreme overestimates. This type of error will occur some of the time since the temperature
156 profiles are based on numerical weather analysis assimilation of temporally and spatially sparse
157 observations. The VZA has little impact here.
158 To examine the impact of cloud microphysics on ΔZ, radiative transfer calculations were
159 performed by applying the Discrete Ordinates Radiative Transfer (DISORT; *Stamnes et al.*
160 [1988]) method to an example case. For a given layer, the layer thickness can be expressed as
161
162 $$\Delta z_i = 4\ \delta\ D_{ei}\ \Delta\tau_i\ /\ 6\ Q\ IWC_i, \qquad (3)$$
163
164 where $\Delta\tau_i$ is the visible optical depth for cloud layer i, the visible extinction efficiency Q has a
165 value of ~2 (e.g., *Minnis et al.* [1998]), IWC_i is the layer ice water content, the density of ice is δ
166 = 0.9 g cm^{-3}, and D_{ei} is the effective diameter of the ice crystals in the cloud layer.

The DISORT calculations assumed an 8.0-km thick cloud extending to 13 km in a tropical atmosphere. The cloud was divided into 198 layers with Δz_i decreasing from less than 110 m at the base to 40 m at the top. The bottom-layer optical depth was specified at 12 to ensure that the cloud is optically thick. Calculations were then performed to compute T_{eff} for a range of IWC and three values of D_e. Three IWC profiles were examined: IWC decreasing linearly from the layer above the base to cloud top, uniform IWC, and IWC increasing from the first layer above the base to the top. The mean IWC of the entire cloud above the bottom layer is the same for all three cases. Z_{eff} was determined from T_{eff} and the simulated cloud-top height correction was computed as 13 km $-Z_{eff}$. The optical depth (IWC) of the layer above Z_{eff}, the top layer, is the sum of τ_i (IWC_i) above Z_{eff}. Figure 3 shows the results for both uniform and decreasing-with-height IWC. Assuming that ~1.5 km of the range in ΔZ (Figure 2a) is due to inaccurate temperature profiles, the observed range is ~4.5 km. That extreme value of ΔZ could occur for D_e = 180 μm and IWC = 0.01 gm^{-3} (Figure 3c) or for smaller values of IWC and D_e (Figure 3b), but is unlikely to occur for very small particles (Figure 3a). The average bias at Z_{eff} = 14 km (Figure 2a) is 2.1 km, a value that can be explained, at VZA = 14°, with uniform or decreasing IWC = 0.014 gm^{-3} and D_e = 80 μm (Figure 3b), or with smaller or larger values of IWC and D_e. For a given value of IWC, ΔZ in Figures a-c is similar for both the uniform and decreasing IWC profiles, except that, for a given ΔZ, the IWC is slightly smaller for the decreasing case. For the increasing-with-height case (not shown), ΔZ rapidly approaches zero with increasing IWC for all particle sizes.

The decreasing-with-height IWC profile is probably most realistic, however, for simplicity, only the uniform IWC case results are considered in the following calculations. Although its value at 5 km is 62 μm, the CERES-MODIS observed mean D_e varies almost

linearly from 55 μm at Z_{eff} = 6 km to 76 μm at 12.6 km, then down to 64 μm at 15 km (not shown). At 14 km, D_e ~ 68 μm, requiring IWC to be ~ 0.011 gm^{-3}. At Z_{eff} = 9 km, ΔZ = 1.6 km and D_e = 68 μm, requiring IWC = 0.019 gm^{-3}. Since the optical depth corresponding to ΔZ is relatively constant (Figure 3d and other IWC cases), IWC can be estimated at each altitude using the proportional relationship

$$\text{IWC} = k\, D_e / \Delta Z, \qquad (4)$$

where ΔZ is determined from Eq (1), D_e is the mean at Z_{eff}, and the proportionality constant k was determined from Eq (4) to be 0.000334 gm^{-3}, using the estimate of IWC for Z_{eff} = 14 km and D_e = 68 μm. Values of uniform IWC were estimated for Z_{eff} = 5 – 15 km and fitted using a third order polynomial regression to obtain

$$\text{IWC} = 0.018 \text{ gm}^{-3} - 0.000474\, Z_{eff}, \qquad (5)$$

where Z_{eff} is in km. The R^2 equals 0.77 indicating that the average IWC is strongly dependent on cloud height. This fit does not apply below 5 km. While the mean IWC varies between 0.01 and 0.02 gm^{-3}, it is somewhat sensitive to the IWC vertical profile and much larger or smaller values of IWC could result from any individual CERES-MODIS/CALIPSO data pair.

The behavior of (5) is not surprising given that IWC has been observed to decrease with decreasing cloud temperature. (T_{eff} was not used as the independent variable here because the height differences were more highly correlated with Z_{eff} than with T_{eff}.) *Heymsfield and Platt* [1984] reported that the mean IWC in cirrus clouds varied from 0.027 gm^{-3} at T = -25°C to 0.001

213 gm^{-3} at -58°C and that IWC variability at a given temperature was typically an order of
214 magnitude or greater. *Wang and Sassen* [2002] found IWC ranging from 0.017 to 0.001 gm^{-3}
215 between -20 and -70°C for comparable clouds. *Garrett et al. [2005]* observed IWCs as large as
216 0.3 gm^{-3} in a thick anvil cloud, while smaller values, ranging from 0.0001 to 0.02 gm^{-3}, were
217 observed by *McFarquhar and Heymsfield* [1996] in the top 2 km of three tropical anvils. The
218 mean IWC values estimated here for the top portions of thick ice clouds are well within the range
219 of observations. The variation in the observed IWC's can also explain much of the random error
220 seen in Figure 2b.

221 Figures 3e and f show that the top-layer τ, constant at ~1.15 for D_e = 80 and 180 μm,
222 increases up to 1.5 for D_e = 10 μm (Figure 3d) and to larger values when IWC < 0.01 gm^{-3}. The
223 corresponding values for the decreasing IWC case are 0.9 and 1.2 for D_e = 80 and 10 μm,
224 respectively, and slightly greater for the increasing IWC case. The values of τ for the larger
225 particles are close to that used by *Sherwood et al.* [2004] to estimate where Z_{eff} should be relative
226 to the lidar-observed top for convective anvils. The difference is mostly due to scattering. Based
227 on the lidar-derived optical depths, *Sherwood et al.* [2004] concluded that the large values of ΔZ,
228 similar to those in Figure 2a, did not correspond to τ =1, but to $\tau \geq 10$. Given the above analysis
229 and the observed range of IWC, it appears that an average value of 2 km for ΔZ is quite
230 reasonable and corresponds to $\tau \sim 1$ for the size of ice crystals retrieved with VISST. For the
231 matched CALIPSO-CERES data used here, the mean height where the CALIPSO beam was
232 fully attenuated is 1.3 km below Z_{eff}, a value much greater than the 150 m calculated for the
233 airborne lidar used in the *Sherwood et al.* [2004] analysis. It is not clear why that earlier analysis
234 produced such different results from the current analysis, but, may be due to assumptions used in

235 the τ retrievals from the airborne lidar or differences in power between it and the CALIOP.
236 Nevertheless, the current results are consistent with the expected values of IWC near cloud top.
237 The optical depths in Figure 3 decrease with VZA as expected. While the small range (9°
238 -19°) in VZA for this study precludes development of an empirical correction for VZA
239 dependence, the plots in Figure 3 suggest a simple cosine variation. Thus, calculating Z_{top}' using
240 either Eq (1) or (2), the VZA-corrected estimate of Z_{top} is
241
242 $$Z_{top} = Z_{eff} + \Delta Z, \qquad (6)$$
243 where $\Delta Z = \mu\ (Z_{top}' - Z_{eff})$. Validating Eq (6) will require a comprehensive combined imager-
244 lidar dataset having a wide range of VZAs.
245
246 **5. Concluding Remarks**
247 The effective cloud radiating height, Z_{eff}, may be adequate for radiative transfer
248 calculations in climate or weather models, but the physical boundaries of a cloud are needed by
249 models to determine where condensates form and persist. The upper boundary is inadequately
250 represented by Z_{eff} for ice clouds. This paper has developed a simple parameterization that uses
251 Z_{eff} to provide, on average, an unbiased estimate of Z_{top} for optically thick ice clouds. It
252 complements the parameterizations used to estimate Z_{top} for optically thin cirrus. The random
253 errors in Z_{top} determined with the new parameterization are consistent with the variations in ice
254 water content observed near cloud top in previous in situ measurements. Reducing the
255 instantaneous uncertainty in Z_{top} may be possible using combinations of different spectral
256 channels or dual-angle views, but the reduction will be limited by the accuracy of the
257 temperature profile. When applied, the parameterization estimate of Z_{top} should have some level

above the tropopause as an upper limit to minimize unrealistic results. If the observed cloud penetrates into the stratosphere, however, Z_{eff} and, hence, Z_{top} can be underestimated because the VISST selects Z_{eff} as lowest the altitude where where T_{eff} is found in the sounding. Additionally, the correction should not be applied to low-level clouds. Although this new parameterization of Z_{top} has been formulated in terms of Z_{eff} determined from the 11-μm brightness temperature, it is probably applicable to Z_{eff} determined using other techniques such as CO_2 slicing. Although only 1 month of CALIPSO data was used here, the results appear robust. Testing with data from other seasons would be required to confirm that contention and data from other satellites, that are not near the CALIPSO ground track, would be needed to verify the formulation for off-nadir angles. With an expanded dataset, it may also be possible to refine the correction in terms of cloud type (e.g., cirrus, anvil, or convective core).

Acknowledgments

This research was supported by NASA through the NASA Energy and Water Cycle Studies Program and the CALIPSO and CERES Projects.

References

Dong, X., P. Minnis, B. Xi, S. Sun-Mack, and Y. Chen (2008), Comparison of CERES-MODIS stratus cloud properties with ground-based measurements at the DOE ARM Southern Great Plains site, *J. Geophys. Res.*, *113*, D03204, doi:10.1029/2007JD008438.

Garrett, T. J., and Co-authors (2005), In situ measurements of the microphysical and radiative evolution of a Florida cirrus anvil, *J. Atmos. Sci. 62*, 2352-2372.

Heymsfield, A. and C. M. R. Platt (1984), A parameterization of the particle size spectrum of ice clouds in terms of the ambient temperature and the ice water content, *J. Atmos. Sci.*, *41*, 846-855.

McFarquhar, G. M. and A. J. Heymsfield (1996), Microphysical characteristics of three anvils sampled during the Central Equatorial Pacific Experiment, *J. Atmos. Sci.*, *53*, 2401-2423.

Minnis, P., D. P. Garber, D. F. Young, R. F. Arduini, and Y. Takano (1998), Parameterizations of reflectance and effective emittance for satellite remote sensing of cloud properties, *J. Atmos. Sci.*, *55*, 3313-3339.

Minnis, P., and Co-authors (2006), Overview of CERES cloud properties from VIRS and MODIS, *Proc. AMS 12th Conf. Atmos. Radiation*, Madison, WI, July 10-14, CD-ROM, J2.3.

Minnis, P., P. W. Heck, and E. F. Harrison (1990), The 27-28 October 1986 FIRE IFO cirrus case study: cloud parameter fields derived from satellite data, *Mon. Weather Rev.*, *118*, 2426-2447.

Minnis, P., and Co-authors (1995), Clouds and the Earth's Radiant Energy System (CERES) algorithm theoretical basis document, volume III: Cloud analyses and radiance inversions (subsystem 4), in *Cloud Optical Property Retrieval (Subsystem 4.3)*, *NASA RP 1376*, vol.3, pp. 135-176.

296 Rossow, W. B. and R. A. Schiffer (1999), Advances in understanding clouds from ISCCP, *Bull.*
297 *Amer. Meteor. Soc.*, *80*, 2261-2287.
298 Sherwood, S. C., J.-H. Chae, P. Minnis, and M. McGill (2004), Underestimation of deep
299 convective cloud tops by thermal imagery, *Geophys. Res. Lett.*, *31*, L11102,
300 doi:10.1029/2004GL019699.
301 Stamnes, K., S. C. Tsay, W. Wiscombe and K. Jayaweera (1988), Numerically stable algorithm
302 for discrete-ordinate-method radiative transfer in multiple scattering and emitting layered
303 media, *Appl. Opt.*, *27*, 2502–2509.
304 Sun-Mack, S., B. A. Wielicki, P. Minnis, S. Gibson, and Y. Chen, 2007: Integrated cloud-
305 aerosol-radiation product using CERES, MODIS, CALISPO, and CloudSat data. *Proc. SPIE*
306 *Europe 2007 Conf. Remote Sens. Clouds and the Atmos.*, Florence, Italy, 17-19 September,
307 *6745*, no. 29.
308 Vaughan, M., Young, S., Winker, D., Powell, K., Omar, A., Liu, Z., Hu, Y., and Hostetler, C.
309 (2004), Fully automated analysis of space-based lidar data: an overview of the CALIPSO
310 retrieval algorithms and data products, *Proc. SPIE*, *5575*, pp. 16-30.
311 Wang, Z. and K. Sassen (2002), Cirrus cloud microphysical property retrieval using lidar and
312 radar measurements. Part II: Midlatitude cirrus microphysical and radiative properties, *J.*
313 *Atmos. Sci.*, *59*, 2291-2302.
314 Winker, D. M., W. H. Hunt, and M. J. McGill (2007), Initial performance assessment of
315 CALIOP, *Geophys. Res. Lett.*, *34*, L19803, doi:10.1029/2007GL03135.
316

Figure Captions

Figure 1. CALIPSO products for 27 April 2007. (a) CALIOP backscatter intensities, (b) CALIPSO feature mask with overlaid CERES-Aqua-MODIS cloud-top heights Z_{top} for single-layer optically thick ice clouds, (c) same as (b) except Z_{top} corrected with Eq (1).

Figure 2. Scatter plots of CALIPSO optically thick non-polar cloud-top altitudes during April 2007 versus (a) Z_{eff} for even days and (b) Z_{top} computed from Z_{eff} using Eq (1) for odd days.

Figure 3. Theoretical variation of (a-c) cloud-top/effective height difference (ΔZ) as function of IWC and (d-f) optical depth of cloud layer above Z_{eff} as function of ΔZ. Main panels are for uniform IWC in the cloud, while insets are for IWC decreasing with increasing height in the cloud.

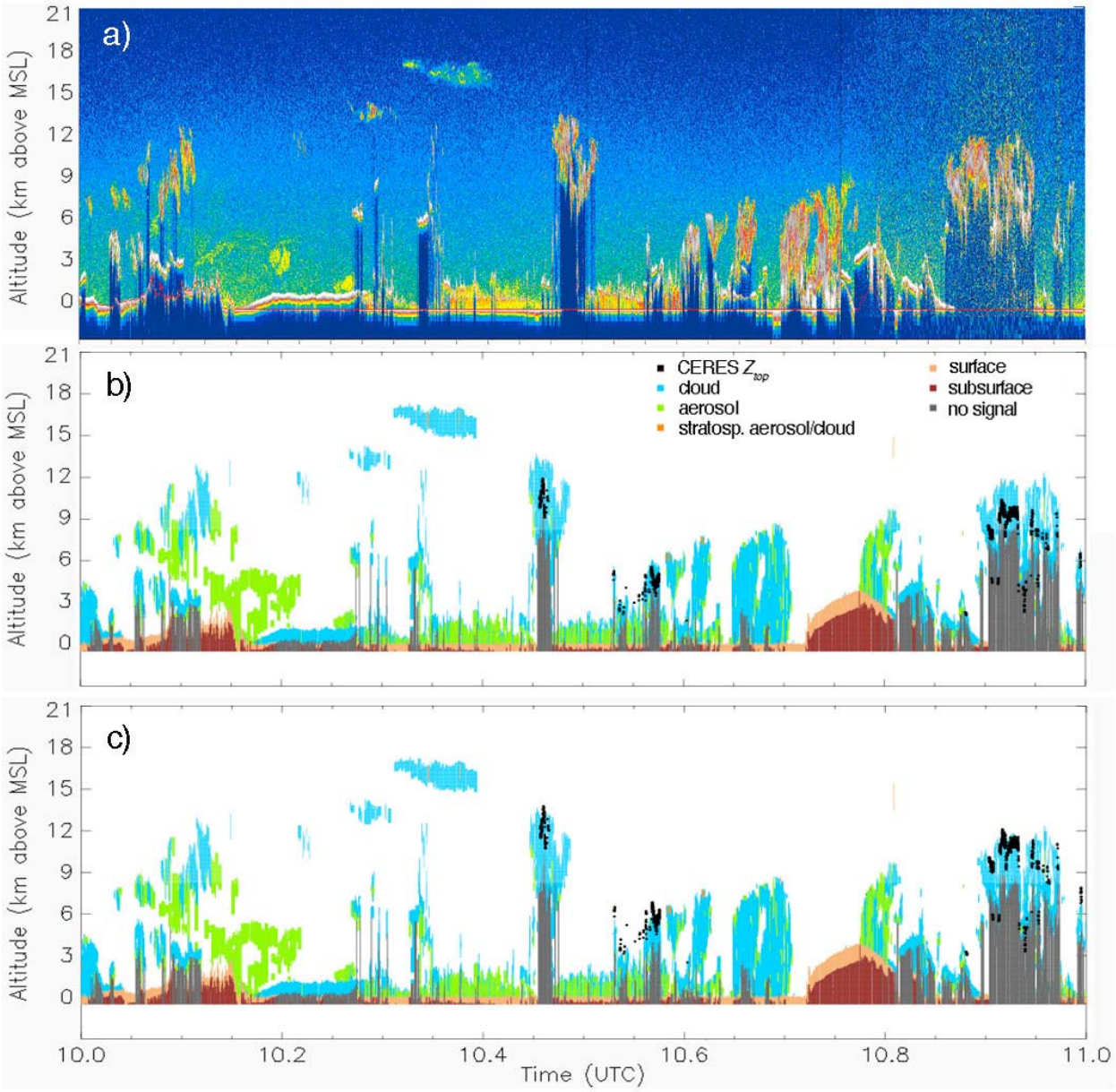

330
331 **Figure 1.** CALIPSO products for 27 April 2007. (a) CALIOP backscatter intensities, (b)
332 CALIPSO feature mask with overlaid CERES Aqua MODIS cloud top heights Z_{top} for single-
333 layer optically thick ice clouds, (c) same as (b) except Z_{top} corrected with Eq (1).
334

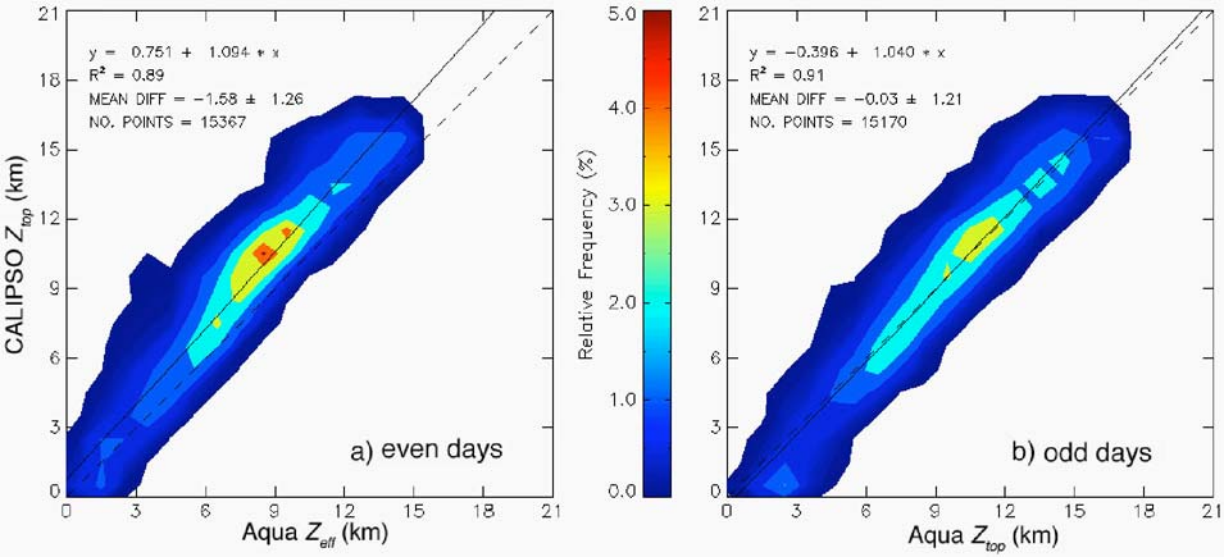

334

335 **Figure 2.** Scatter plots of CALIPSO optically thick non-polar cloud top altitudes during April

336 2007 versus (a) Z_{eff} for even days and (b) Z_{top} computed from Z_{eff} using Eq (1) for odd days.

337

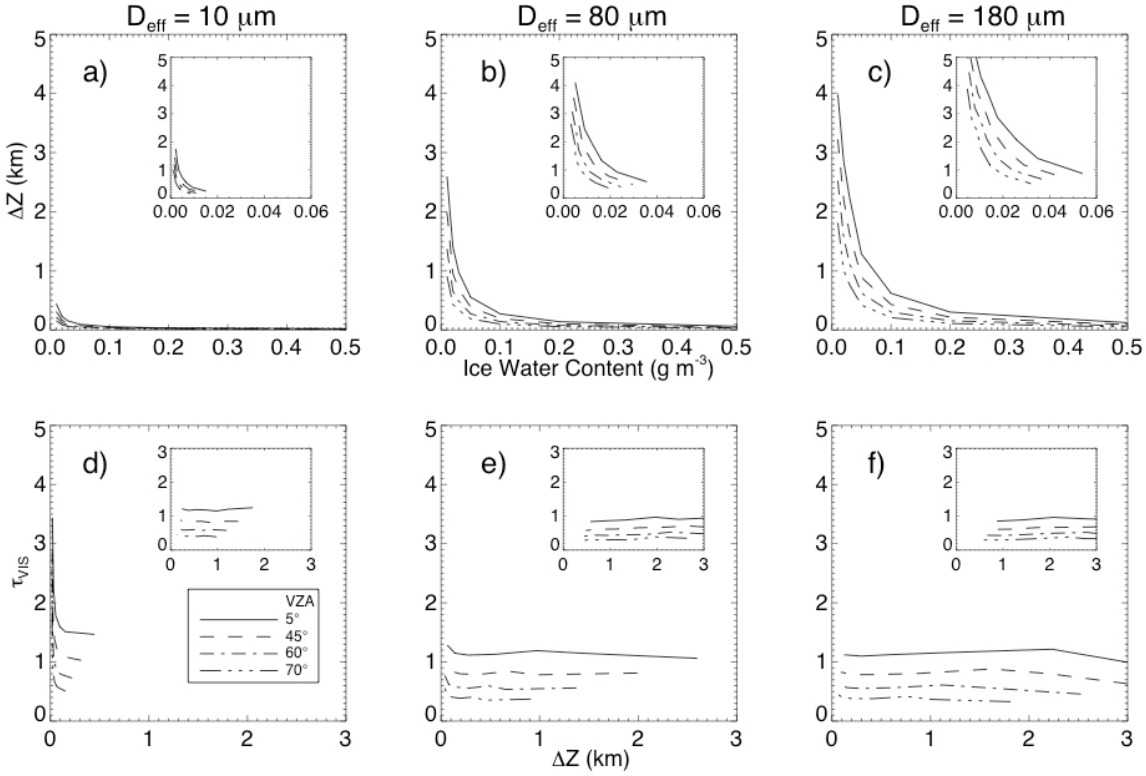

337

338 **Figure 3.** Theoretical variation of (a-c) cloud-top/effective height difference (ΔZ) as function of

339 IWC and (d-f) optical depth of cloud layer above Z_{eff} as function of ΔZ. Main panels are for

340 uniform IWC in the cloud, while insets are for IWC decreasing with increasing height in the

341 cloud.

342